OXFORD

JNCI J Natl Cancer Inst (2018) 110(9): djy011

doi: 10.1093/jnci/djy011
First published online February 28, 2018
Article

ARTICLE

Role of Acid Sphingomyelinase and Ceramide in Mechano-Acoustic Enhancement of Tumor Radiation Responses

Ahmed El Kaffas*, Azza Al-Mahrouki*, Amr Hashim, Niki Law, Anoja Giles, Gregory J. Czarnota

See the Notes section for the full list of authors' affiliations.
Correspondence to: Gregory J. Czarnota, PhD, MD, FRCPC, 2075 Bayview Avenue, Room T2-185, Toronto, ON, Canada, M4N 3M5 (e-mail: gregory.czarnota@sunnybrook.ca).
*Authors contributed equally to this work.

Abstract

Background: High-dose radiotherapy (>8–10 Gy) causes rapid endothelial cell death via acid sphingomyelinase (ASMase)–induced ceramide production, resulting in biologically significant enhancement of tumor responses. To further augment or solicit similar effects at low radiation doses, we used genetic and chemical approaches to evaluate mechano-acoustic activation of the ASMase-ceramide pathway by ultrasound-stimulated microbubbles (USMB).
Methods: Experiments were carried out in wild-type and acid sphingomyelinase (*asmase*) knockout mice implanted with fibrosarcoma xenografts. A cohort of wild-type mice received the ASMase-ceramide pathway inhibitor sphingosine-1-phosphate (S1P). Mice were treated with varying radiation doses, with or without a priori USMB exposure at different microbubble concentrations. Treatment response was assessed with quantitative 3D Doppler ultrasound and immunohistochemistry at baseline, and at three, 24, and 72 hours after treatment, with three to five mice per treatment group at each time point. All statistical tests were two-sided.
Results: Results confirmed an interaction between USMB and ionizing radiation at 24 hours ($P < .001$), with a decrease in tumor perfusion of up to 46.5% by three hours following radiation and USMB. This peaked at 24 hours, persisting for up to 72 hours, and was accompanied by extensive tumor cell death. In contrast, statistically nonsignificant and minimal tumor responses were noted in S1P-treated and *asmase* knockout mice for all treatments.
Conclusions: This work is the first to confirm the involvement of the ASMase-ceramide pathway in mechanotransductive vascular targeting using USMB. Results also confirm that an acute vascular effect is driving this form of enhanced radiation response, and that it can be elicited at low radiation doses (<8–10 Gy) by a priori USMB exposure.

In conventional radiobiology, ionizing radiation (XRT) is known to act by inducing DNA strand breaks (1). Tissue radiation responses are generally associated with the inherent radiosensitivity of populating cells. Recent research has challenged this canonical notion, demonstrating that endothelial cells are a regulator of high-dose radiation response (2–8).

The role of endothelial cells as radiation response regulators is linked to the apoptosis second messenger ceramide (8). Evidence suggests that single doses of radiation (>8–10 Gy) act on endothelial membranes and cause hydrolyzation of sphingomyelin into ceramide via acid sphingomyelinase enzymes (ASMase), and consequent downstream rapid endothelial apoptosis (9). In contrast, conventional low doses (<6 Gy), commonly utilized in fractionated regimens, functionally result in no biologically active production of ceramide (8). Pretreating endothelial cells with sphingosine-1-phosphate (S1P) minimizes ceramide-induced cell death (10). Similarly, *acid sphingomyelinase* gene (*asmase*) knockout mice are more resistant to high-

Received: September 18, 2016; **Revised:** November 16, 2017; **Accepted:** January 16, 2018

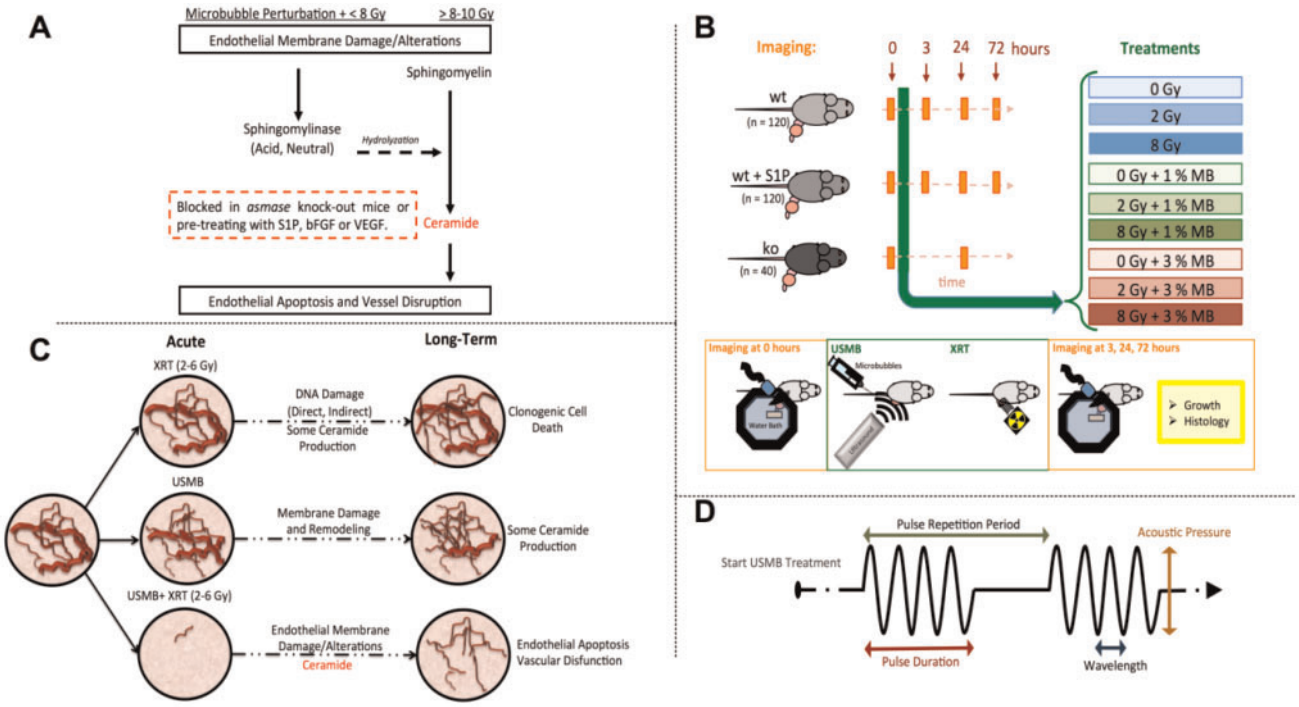

Figure 1. Overview of hypothesis and method schematics. **A)** Hypothesized biological mechanism behind ultrasound-stimulated microbubbles (USMB) and radiation treatments involving acid sphingomyelinase (ASMase) and ceramide. Whereas high doses (>8 Gy) of radiation alone activate sufficient ceramide to message for endothelial cell death, radiation doses lower than 2–6 Gy do not release sufficient quantities to activate ceramide-induced cell death. Similarly, whereas ceramide is released following USMB treatments, the amount is not sufficient to activate the rapid and extensive endothelial cell death needed for vascular shutdown. In contrast, combining radiation (low or high dose) with USMB releases sufficient ceramide to surpass the threshold, resulting in extensive tumor endothelial cell death and vascular shutdown. Because the microbubbles used have an average diameter of 3 μm and thus remain within blood vessels, treatment with USMB mechanically targets endothelial cells that surround the flowing intravascular microbubbles. **B)** Schematic of experimental conditions and imaging and treatment workflow. **C)** Hypothesized therapeutic mechanism following USMB and radiation treatments. In tissues, we posit that the combined USMB and radiation treatment causes vascular perturbation, a disruption in blood flow, and changes in oxygenation, leading to cell death, consistent with what appears to be potentially ischemic tumor cell death. The rationale behind the approach is that areas with induced anoxic cell death do not require any further therapeutic doses of radiation due to the massive vascular destruction already caused by an initial USMB and radiation treatment (12,32,33). **D)** Schematic of treatment pulse used to stimulate microbubbles (total USMB treatment time was five minutes, with 16-cycle tone burst, 3 kHz pulse repetition frequency, duty cycle of 10%, peak negative acoustic pressure of 500 kPa, mechanical index of 0.8). ko = knockout; MB = microbubble; S1P = sphingosine-1-phosphate; USMB = ultrasound-stimulated microbubble; wt = wild-type; XRT = ionizing radiation.

dose radiation treatments than wild-type mice (2,3). Correspondingly, mechanical forces exerted on endothelial membranes can promote survival or death via mechanotransduction of ceramide (11).

Recent investigations have demonstrated in preclinical models of human tumors that ultrasound-stimulated microbubbles (USMB) can mechanically perturb cell membranes, resulting in a hypothesized mechanotransductive ceramide-based radiation enhancement event (12–14). The radiosensitization process takes advantage of the known sensitivity of endothelial cell membranes to mechanical forces and results in a synergistic interaction between physical effects on endothelial cells and radiation effects at both low (<6 Gy) and high (>8 Gy) doses (12,13,15–21).

The purpose of this study was to investigate the role of ASMase-ceramide mechanotransduction through USMB for radiation enhancement using genetic and chemical approaches. The hypothesis is that single doses of radiation combined with USMB will abruptly disrupt tumor perfusion in wild-type mice, but will be minimally effective in mice pretreated with S1P or in *asmase* knockout mice. Investigations were carried out to determine acute responses of the vascular and cellular components of tumors following 2 Gy or 8 Gy irradiation and USMB doses.

Methods

Tumor Model

All experiments were conducted in compliance with internationally recognized guidelines specified in protocols approved by the Sunnybrook Research Institute institutional animal care committee (protocol No. 351). Experiments aimed at elucidating the role of ASMase and ceramide in acoustic radiosensitization of tumor endothelium (Figure 1, A and C). MCA-129 fibrosarcoma cells were injected in the right hind leg of wild-type (wt) or *asmase* knockout (ko) mice. The mice (n = 603) were bred from heterozygous *asmase* +/+ or −/− genotyped breeders (Figure 1B) (3).

Treatment

All mice were anesthetized with subcutaneous ketamine and xylazine injection prior to experiments. Radiation-treated mice received a single dose of 2 or 8 Gy to tumor. A subset of wild-type mice received 0.1 mg S1P intravenously 30 minutes prior to treatment (22,23). For USMB, mice were jig-mounted and partially submerged to place tumors within the range of a 500 kHz transducer (24). Microbubbles (Definity, Lantheus Medical

ARTICLE

Imaging, N. Billerica, MA) were diluted in saline (25 μL in 75 μL of saline for 1% "low" doses; 70 μL in 30 μL of saline for 3% "high" doses) and intravenously tail vein–injected during insonification. Microbubbles were stimulated within tumor volumes (Figure 1D). For each time point, three to five mice were used per treatment group. See the Supplementary Materials (available online) for details.

In Vivo Imaging

High-frequency 3D power Doppler was acquired (0, 3, 24, 72 hours; 0, 24 hours for knockout) using a VEVO770 (Visualsonics, Toronto, ON, Canada) with a 30 MHz transducer (6,21,25–28). Analysis was conducted using in-house developed software (MATLAB, The MathWorks, Natick, MA) to compute the vascularity index (VI) (6). The relative VI was used to quantitatively assess perfusion changes. These data were normalized per mouse, comparing the volume of grouped colored pixels in the selected region of interest per whole tumor after treatment with similar regions before treatment $((VI_{After}/ VI_{Before}) \times 100) - 100)$. See the Supplementary Materials (available online) for details.

Immunohistochemistry, Ceramide Detection, Enzyme-Linked Immunosorbent Assay, and Tumor Growth Assessment

Mice were killed at three, 24, and 72 hours, and 5 μm thick tumor slices were stained with in situ end labeling (ISEL) or cluster of differentiation 31 (CD31). ISEL sections were quantified by obtaining a ratio of stained areas to tumor area. Microvascular densities (MVDs) were quantified from CD31 sections (MVD) (29). Ceramide staining and quantification were conducted by counting the proportion of ceramide-stained endothelial cells. ASMase and ceramide synthase 1 (CS1) were quantified from the plasma of mice, and ceramide kinase was quantified from tumor tissues, using enzyme-linked immunosorbent assay (ELISA). Ceramide was measured using mass spectrometry. Tumor growth was measured two to three times per week for up to 20 days. See the Supplementary Material (available online) for details.

Statistical Analysis

Quantified parameters (VI, MVD, and cell death) were analyzed statistically using a two-way analysis of variance (ANOVA) to test for main effects and dose-dependent interaction of radiation and USMB at each time. Pairwise multiple comparisons were performed using Tukey's Honest Significant Difference Procedure to test for statistical significance between conditions and associated control conditions in respective genotypes (wt, S1P, or ko) at each time (30,31). A three-way ANOVA was used to test for an overall radiation-by-USMB-by-time interaction. Statistical means, confidence intervals (CIs), number of mice (n), and *P* values are summarized in Supplementary Tables 1–3 (available online). Ceramide quantification was compared with control conditions using an unpaired two-tailed *t* test. Statistical analyses were done in MATLAB (The MathWorks, Natick, MA) and Prism (GraphPad, La Jolla, CA). All statistical tests were two-sided, and a *P* value of less than .05 was considered statistically significant.

Results

Vascular Effects of Radiation and USMB

Representative maximum intensity projection volumes of tumor blood flow, depicted with 3D Doppler, are presented in Figure 2. The top rows of Figure 2, A and B, qualitatively exhibit Doppler signal decreases by 24 hours, sustained for up to 72 hours (Figure 2C) following single doses of radiation alone (Figure 2A), or in conjunction with USMB (Figure 2B), in wild-type mice. In contrast, data from S1P-treated mice (second row in Figure 2A) suggest no decreases in Doppler signal following radiation alone, or when combined with USMB. The quantified relative VI is presented at three, 24, and 72 hours after single-dose radiation therapy and/or USMB in Figure 2, C and D (Supplementary Tables 1 and 2, available online). ANOVA of the relative VI indicated a statistically significant interaction between radiation and USMB at 24 hours ($P < .001$), with a statistically significant ($P < .001$) acute (within 3 hours) decrease (SD) of up to 46.5% (16.6%) in the VI. At 24 hours, only combinations of low and high USMB with 2 ($P = .01$) or 8 ($P < .001$) Gy radiation were statistically significant.

Mice where sphingosine-1-phosphate was used as an inhibitor of ceramide had no notable blood flow diminishment following radiation when delivered alone, or when combined with USMB exposure. For example, at 24 hours following treatment, a single dose of 8 Gy radiation alone diminished detectable blood flow (VI) by –30.3% (4.5%), and exposure to low USMB increased blood flow by 18.1% (13.1%), whereas the combination of the two treatments statistically significantly ($P < .001$) diminished blood flow to –58.8% (13.9%) of the original detected flow. In the presence of S1P, no statistically significant changes in blood flow were observed (Supplementary Table 2, available online).

Figure 3, A and B, and Supplementary Figure 1 (available online), present images of representative CD31-stained tumor cross-sections demonstrating that vascular density diminished in response to radiation and/or USMB exposure. Corresponding quantified results presented in Figure 3, C and D, were in agreement (Supplementary Tables 1 and 2, available online). For instance, the control sample CD31 MVD (SD) was 130 (27) at 24 hours post-treatment. In contrast, it was observed to be 83 (22) for mice treated with a single dose of 8 Gy, 119 (37) for those treated with 1% USMB (low) alone, and 40 (32) for mice treated with combined treatments of 8 Gy and low USMB. In the presence of S1P, this was minimally changed relative to controls.

Tumor Cell Death Assessment Following Radiation and USMB

Figure 4A exhibits images of representative ISEL-stained tumor cross-sections from 0, 2, and 8 Gy treated mice with and without low or high USMB, at three, 24, and 72 hours. High-magnification images of all ISEL-stained tumor cross-sections are presented in Supplementary Figure 2 (available online). Quantification is presented in Figure 4, C and D, and Supplementary Tables 1 and 2 (available online). From these, an increase in cell death was observed in wild-type mice, peaking at 24 hours. Whereas control (0 Gy, 0% USMB in wild-type mice) mean levels of cell death ranged from 5% to 10% over time, samples treated with combined low USMB and 8 Gy radiation resulted in cell death increases (SD) of 8.7% (6.0%), 53.2% (24.3%), and 37.8% (22.5%) at three, 24, and 72 hours, respectively. Radiation alone (8 Gy) resulted in cell death levels (SD) of 10.0%

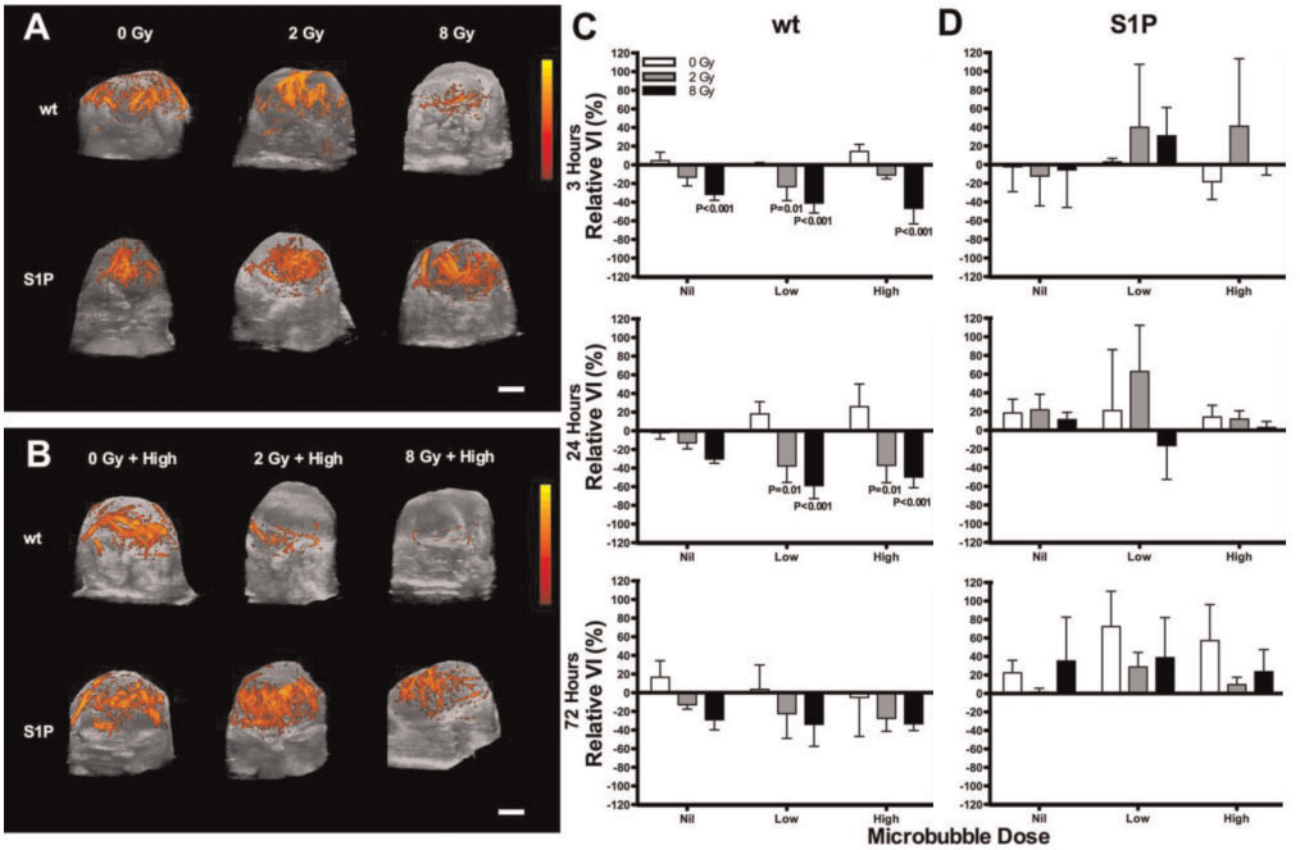

Figure 2. Power Doppler results. **A and B)** Tumor results of maximum intensity projections of the power Doppler signal in volumetric images for various treatment conditions. The **scale bar** is 2 mm, and the **color bar** is 0 (**black**) to 40 dB (**yellow**). **A and B)** Results 24 hours after treatment with radiation alone, and radiation in combination with ultrasound-stimulated microbubble (USMB) exposure, respectively. **C and D)** Quantified relative vascularity index at three hours, 24 hours, and 72 hours for each of the radiation and USMB (low is 1%, and high is 3% volume of total blood volume [v/v]) treatment conditions in wild-type (wt) and sphingosine-1-phosphate (S1P)-treated mice. The three- and 72-hour time points have four mice per treatment; the 24-hour time has five mice per treatment. Pairwise multiple-comparisons were performed using two-sided Tukey's Honest Significant Difference Procedure to test for statistical significance following analysis of variance. All *P* values are displayed for statistically significant treatment conditions in the graph. All statistical comparisons are compared with the 0 Gy, 0% ultrasound-stimulated microbubbles (Nil) condition at the same time and are summarized in Supplementary Tables 1 and 2 (available online). **Error bars** represent SD. S1P = sphingosine-1-phosphate; wt = wild-type; VI = vascularity index.

ARTICLE

(7.9%), 17.3% (10.6%), and 15.4% (9.8%), at three, 24, and 72 hours, respectively. Low USMB treatment alone resulted in 11.2% (8.8%), 5.2% (5.0%), and 20.0% (6.6%) cell death at three, 24, and 72 hours, respectively (Figure 4C). Mice treated in advance with S1P expressed minimal cell death, as quantified from ISEL-stained tumor cross-sections (Figure 4, B and D).

Radiation and USMB Effects in *asmase* Knockout Mice

Results from experiments with *asmase* knockout mice, evaluated 24 hours after treatments, are presented in Figure 5 and Supplementary Table 3 (available online). Overall, the relative VI followed a similar trend to S1P-treated mice; there was no statistically significant decrease observed at any radiation dose used. For instance, in wild-type mice, the VI changed by 18.1% (13.1%), –37.7% (17.7%), and –58.8% (13.9%) at 24 hours following treatments with low USMB and 0, 2, or 8 Gy radiation, respectively. In contrast, it changed by 35.5% (45.5%), 28.9% (28.9%), and 11.6% (10.6%) for the same treatments, respectively, in knockout mice (Figure 5D). Knockout mice were also resistant to the effects of radiation or USMB alone. As anticipated, CD31 and ISEL results also indicated minimal vascular effects and minimal cell death in knockout mice (Figure 5, E and F). ANOVA demonstrated no statistically significant dose effect in knockout CD31 and ISEL results.

Endothelial Ceramide Production and Tumor Growth Delay in Wild-type, S1P-Treated, and *asmase* Knockout Mice Exposed to Radiation and USMB

Ceramide staining results at 24 hours for wild-type, S1P-treated, and *asmase* knockout mice exposed to 8 Gy and/or high USMB treatment are presented in Figure 6, A and B, and Supplementary Figure 3A (available online). This dose was selected for experimentation given its maximal ceramide production in experiments here. Qualitatively, images demonstrated an increase in ceramide only in radiation and/or USMB-treated wild-type mice. Minimal staining was observed in S1P-treated or *asmase* knockout mice. Quantification of ceramide is presented as a difference relative to the 0 Gy, 0% USMB (Nil) condition at the corresponding time (24 hours) (Figure 6B). Ceramide staining was only statistically significant for wild-type mice receiving radiation with USMB, with a percent vessel staining (SD) for ceramide at 0.8% (0.3%; $P = .04$). In

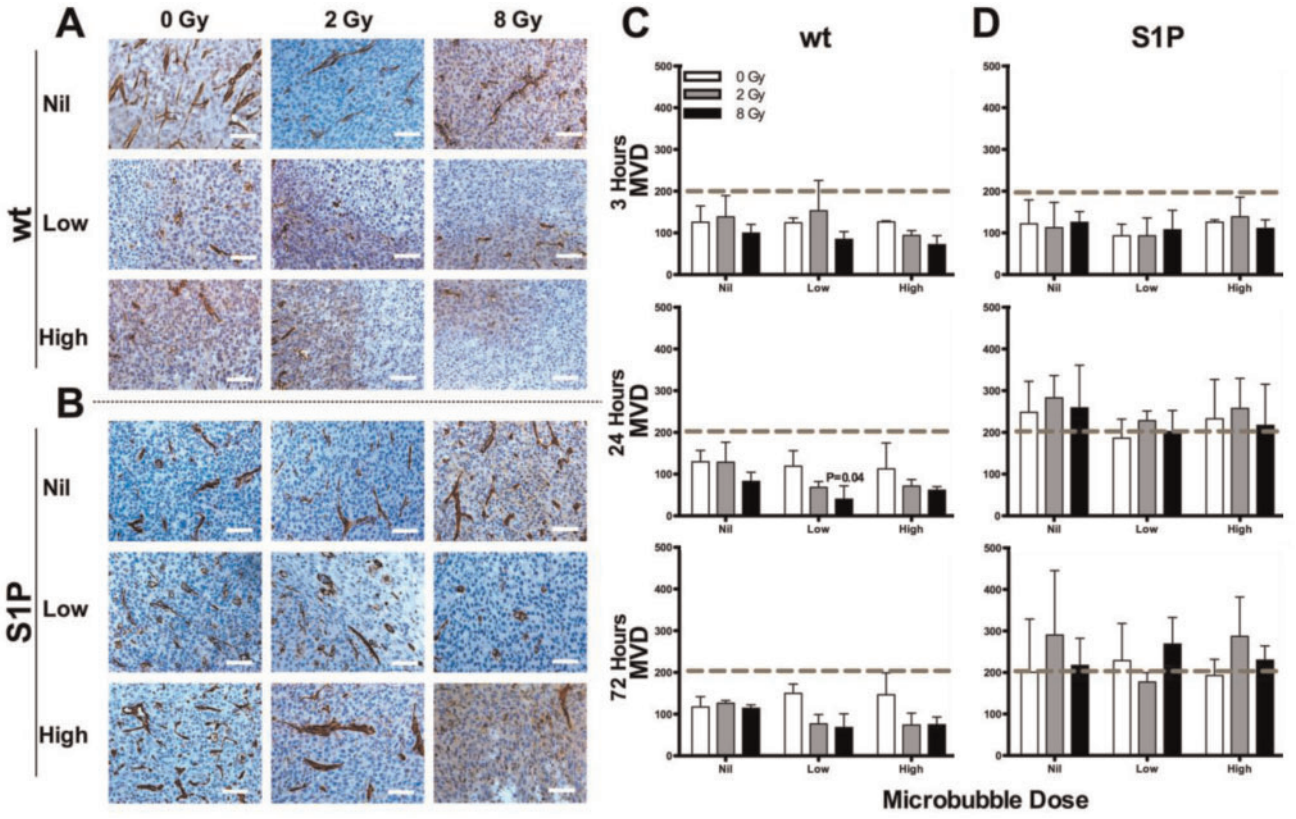

Figure 3. Cluster of differentiation 31 (CD31) results. **A and B)** Representative images of CD31-stained tumor sections from wild-type (wt) and sphingosine-1-phosphate (S1P)-treated mice following radiation and ultrasound-stimulated microbubble (USMB; low is 1%, and high is 3% volume of total blood volume [v/v]). The **scale bar** represents 50 μm. **C and D)** Quantified CD31 staining for all radiation doses and time points in wild-type (wt) and S1P-treated mice. The following wt treatment conditions have three mice each: all 3% USMB at three hours; all 1% or 3% USMB at 72 hours. All other wt treatment conditions have four mice each. The following S1P treatment conditions have three mice each: all 1% USMB at three hours; 3% USMB with 2 Gy at three hours; 2 Gy only; 1% USMB with 0 Gy and 2 Gy at 24 hours; control at 72 hours; 1% USMB with 2 Gy at 72 hours. All other S1P treatment conditions have four mice each. Pairwise multiple comparisons were performed using two-sided Tukey's Honest Significant Difference Procedure to test for statistical significance following analysis of variance. All *P* values are displayed for statistically significant treatment conditions. All statistical comparisons are compared with the 0 Gy, 0% ultrasound-stimulated microbubbles (Nil) condition at the same time and are summarized in Supplementary Tables 1 and 2 (available online). **Error bars** represent SD. MVD = microvascular density; S1P = sphingosine-1-phosphate; wt = wild-type.

contrast, *asmase* knockout mice had the lowest level of ceramide per vessel, ranging from –0.4% to <0.01%, over all treatment conditions, in comparison with the control (0 Gy and 0% USMB) mice of <0.01 ± 0.01%. Mass spectrometry results indicated an elevation in ceramide species relative to controls most pronounced at three hours (Supplementary Figure 4A, available online). In S1P-treated mice, there was elevation of some ceramide species within three hours of USMB alone, or when combined with radiation, but not for radiation alone. These were attenuated 24 hours after treatments (Supplementary Figure 4B, available online). Additionally, quantified ceramide synthase in plasma increased the most for the USMB and radiation-treated mice at both three and 24 hours after treatment in wild-type mice. Similarly, plasm ASMase increased the most in USMB and radiation-treated mice at three and 24 hours after treatment in wild-type mice, and remained relatively similar following S1P exposure (Supplementary Figure 5A, available online). Ceramide kinase expression increased most in knockout mice following combined USMB and radiation at 24 hours (Supplementary Figure 5B, available online). Tumor growth delay results are presented in Figure 6, which were consistent with effects being ceramide production dependent.

Statistical Analysis

Two-way ANOVA with testing for main effect and interaction was conducted for all power Doppler, CD31, and ISEL data (Supplementary Tables 1–3, available online). This was conducted for wild-type, S1P-treated mice and *asmase* knockout mice used in experiments. Results from ANOVA indicated effects that were consistent with our previous work, with an interaction between ultrasound-stimulated microbubbles and radiation. This has been observed with PC3 tumors (prostate tumor line), MB-231 tumors (breast tumor line), and bladder tumors (HT1376) (reviewed in [13,32]). Those studies similarly demonstrated differences in CD31, ISEL/TUNEL staining, and power Doppler data between microbubble-stimulated ultrasound and radiation treatments in comparison with treatments with single modalities alone (ultrasound-stimulated microbubbles alone or radiation alone). There were differences in the time at which effects were most prominent, and differences in the extent of effect, that may be related to the extent of tumor vasculature. The results in the study here demonstrated an interaction between USMB and XRT in terms of a main effect and also indicated an interaction with statistical significance that was most prominent at 24 hours for power Doppler data. By 72

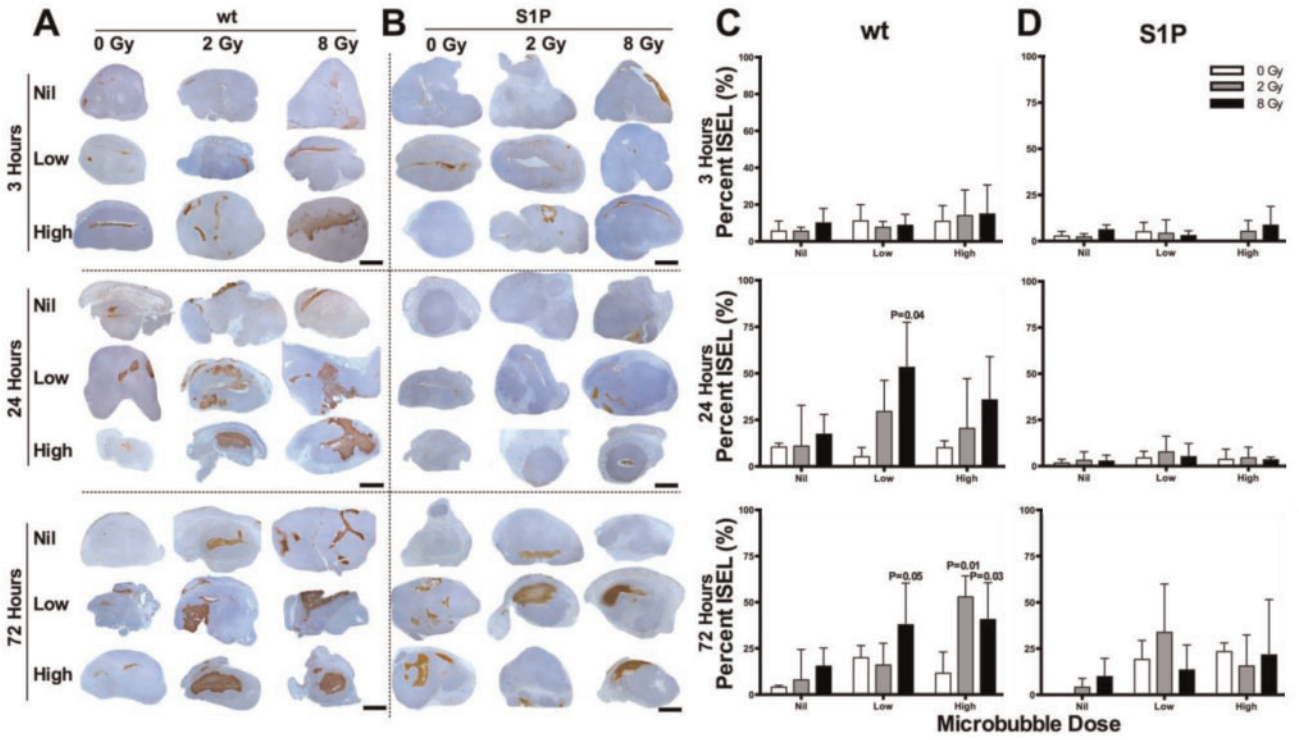

Figure 4. Tumor cell death results. **A and B)** Representative images of in situ end labeling (ISEL)–stained tumor cross-sections from wild-type (wt) and sphingosine-1-phosphate (S1P)-treated mice following ultrasound-stimulated microbubbles (USMB; low is 1%, and high is 3% volume of total blood volume [v/v]) and radiation. The **scale bar** represents 1 mm. **C and D)** Quantified ISEL staining for all radiation doses and time points in wild-type and S1P-treated mice. All wt treatment conditions include four mice each, except for radiation-only conditions at 72 hours. All S1P treatment conditions include four mice each. Pairwise multiple comparisons were performed using two-sided Tukey's Honest Significant Difference Procedure to test for statistical significance following analysis of variance. All *P* values are displayed for statistically significant treatment conditions. Statistical comparisons are compared with the 0 Gy, 0% USMB (Nil) condition at the same time point and are summarized in Supplementary Tables 1 and 2 (available online). **Error bars** represent SD. ISEL = in situ end labeling; S1P = sphingosine-1-phosphate; wt = wild-type.

hours, changes were less prominent. There was an effect of time noted, with statistical significance. There were effects noted for USMB and XRT as well as for CD31 data at 24 hours. A main effect and an interaction were also noted with statistical significance that persisted to 72 hours. ISEL data indicated main effect and interaction, which persisted to 72 hours (Supplementary Table 1–3, available online).

These effects were absent for all experiments conducted in the presence of S1P for power Doppler, CD31, and ISEL. Similarly, effects were absent in experiments conducted for knockout mice for power Doppler, CD31, and ISEL. See Supplementary Table 2 and Supplementary Table 3, respectively (available online).

Discussion

The work here demonstrates for the first time, using genetically modified mice, that activation of the ASMase-ceramide molecular pathway following USMB exposure is necessary for radiosensitization. Experiments were conducted in wild-type, as well as chemically treated and genetically modified endothelial apoptosis-resistant mice (*asmase* knockout). Statistically significant vascular shutdown was detectable by three hours following USMB and radiation treatments, with up to 40% Doppler signal decreases. Vascular shutdown peaked at 24 hours, persisted for up to 72 hours, and was directly linked to increases in tumor cell death when radiation and USMB were combined. A statistically significant interaction between USMB and radiation was observed at 24 hours, indicating that both of these treatments act together to induce the vascular response. In contrast, minimal responses were noted in *asmase* knockout or S1P-treated mice. Results reinforce previously reported interactions between radiation and USMB (13,33) and confirm the involvement of ASMase and ceramide in endothelial radiosensitization.

The proposed therapeutic approach enhances radiation above and beyond radiosensitizing chemical agents by targeting mechanotransductive effects that invoke ceramide (Figure 1, A and C). Endothelial cells are an ideal target because they have a 20-fold enrichment of a nonlysosomal secretory form of ASMase in comparison with epithelial cells, thus resulting in greater ceramide production (34). Our results, which include quantified ceramide assays using mass spectrometry and ELISA, support this.

Dose-dependent radiation effects were examined. We anticipated that only high radiation doses (8 Gy) would produce sufficient ceramide to cause rapid endothelial apoptosis (8). We also expected that low doses of radiation administered with USMB would augment the 2 Gy radiation effect. Here, we confirmed this and found nearly similar tumor vascular shutdown following combined 2 Gy with USMB treatment, or a single high dose of 8 Gy. Thus, USMB enables radiation effects on vasculature and blood flow at single 2 Gy radiation doses.

The effects of low- and high-concentration microbubble therapy were examined. Although both resulted in vascular shutdown when combined with radiation, superior effects were

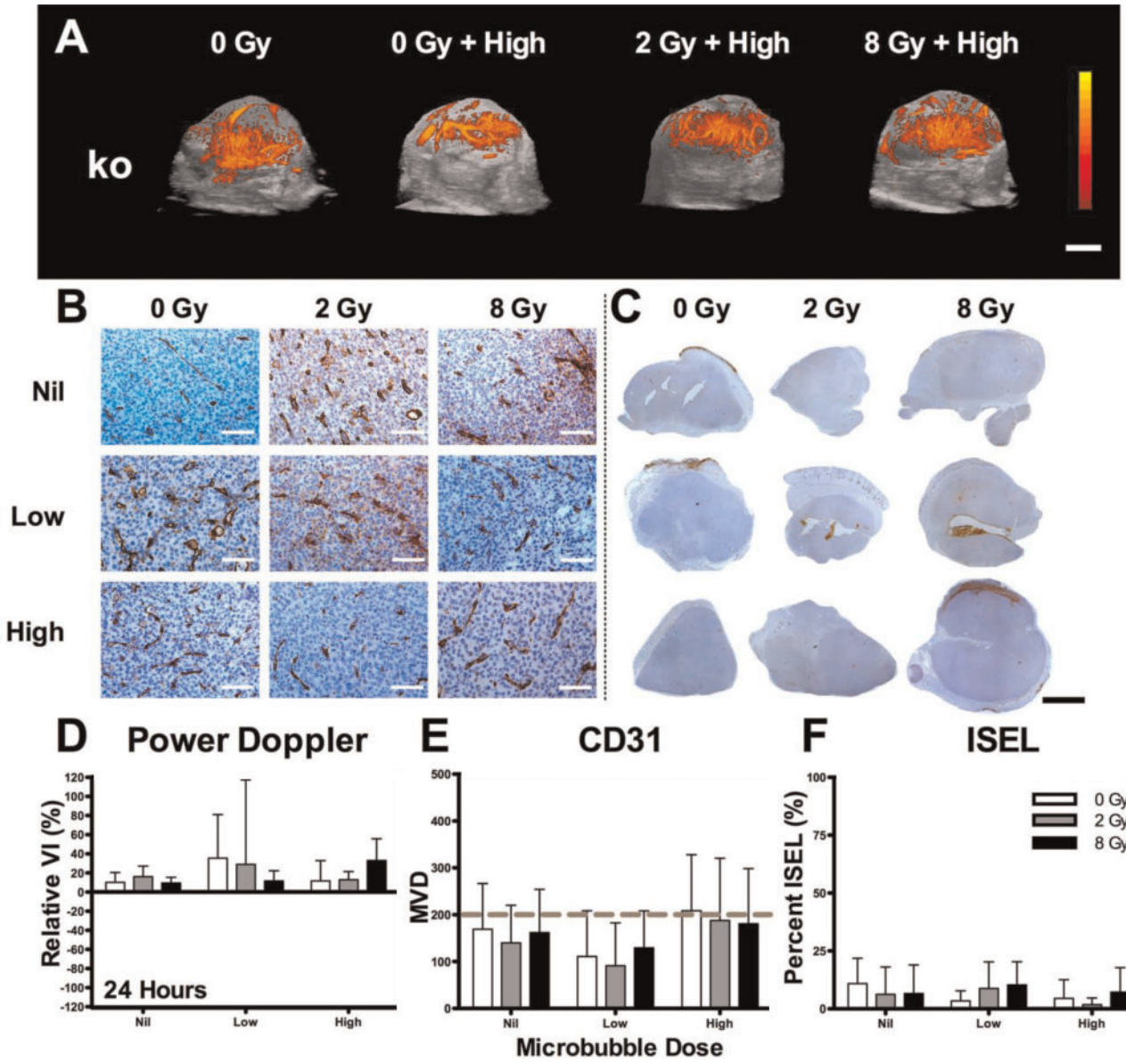

Figure 5. Power Doppler and histological results for wild-type (wt) and asmase knockout mice at 24 hours after irradiation. **A)** Representative results of maximum intensity projections of the power Doppler signal in volumetric images for various treatment conditions. The **scale bar** is 2 mm, and the **color bar** is 0 (**black**) to 40 dB (**yellow**). The **scale bar** represents 1 mm. **B)** Representative images of cluster of differentiation (CD31)–stained tumor sections from wild-type and knockout mice following radiation and ultrasound-stimulated microbubbles (USMB; low is 1%, and high is 3% volume of total blood volume [v/v]). The **scale bar** is 60 μm. **C)** Representative images of in situ end labeling (ISEL)–stained tumor cross-sections from wild-type (wt) and knockout (ko) mice following USMB and radiation. The **scale bar** is 1.3 mm. **D–F)** Quantified power Doppler, CD31, and ISEL results for wild-type and knockout mice. All ko treatment conditions in **(D–F)** have five mice each. Pairwise multiple comparisons were performed using two-sided Tukey's Honest Significant Difference Procedure to test for statistical significance following analysis of variance. All *P* values are displayed for statistically significant treatment conditions. All statistical comparisons are compared with the 0 Gy, 0% USMB (Nil) condition at the same time point and are summarized in Supplementary Table 3 (available online). **Error bars** represent SD. ISEL = in situ end labeling; MVD = microvascular density; VI = vascularity index.

noted in mice treated with radiation and high USMB. Intriguingly, increases in flow were noted in mice treated with USMB alone. These may be triggered by remodeling of blood flow due to shutdown of smaller tumor capillaries (immature endothelial cells that may be more sensitive), and subsequent flow increases in the larger tumor vessels (6,35–37).

Statistical analyses included two-way ANOVA and descriptive statistics. Qualitatively, while a relative VI trend over time was noted, this did not appear linear. Upon testing for a time interaction using a three-way ANOVA, only a marginally statistically significant interaction was identified in wild-type mice. Thus, we focused on testing interactions within each imaging time point using a two-way ANOVA. Overall, experiments were balanced for breadth and scope against practicality in determining each condition's sample size. In our experience with the effect being detected (perfusion changes, cell death), this number is sufficient for statistical significance. Future experimentation of more subtly different conditions will require larger mice subsets.

A previous study has tied cell membrane metabolism gene activation with endothelial exposure to USMB and confirmed upregulation of genes related to membrane remodeling, damage,

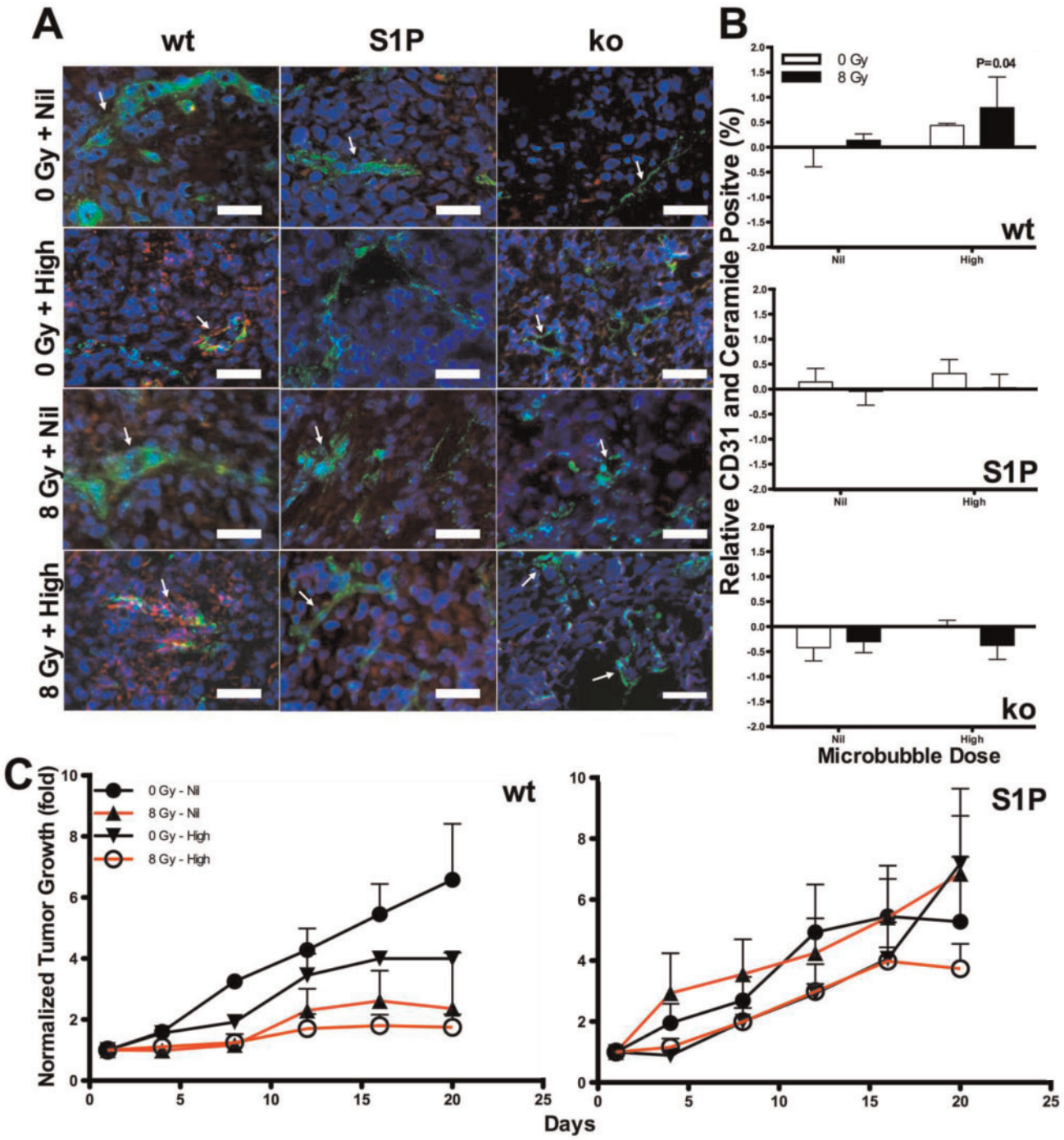

Figure 6. Ceramide staining and tumor growth in wild-type and S1P-treated mice. **A)** Tumor sections triple labeled for ceramide (red), endothelial cells (cluster of differentiation [CD31]; green), and cellular nuclei (double stranded DNA [DAPI]; **blue**). Ceramide (**red fluorescence**) is elevated in treated wild-type (wt) mice; minimal ceramide is noted in sphingosine-1-phosphate (S1P) and knockout (ko) mice. **Arrows** point to the labeling of endothelial cells lining blood vessels (CD31 labeling, **green fluorescence**) that appear **yellowish-orange** in treated wt due to the overlay of the **red** (ceramide) and the **green** (CD31); DAPI is a nuclear stain (**blue fluorescence**). The **scale bar** is 20 μm. **B)** Quantified ceramide for wild-type, S1P, and knockout mice. Each treatment condition has four mice. **Error bars** represent SEM. **C)** Tumor growth normalized to baseline for wild-type and S1P mice treated with high ultrasound-stimulated microbubbles (USMB; high is 3% volume of total blood volume [v/v]) and ionizing radiation (8 Gy). For wt growth curves, there are 10 mice in the control group, eight mice in the 8 Gy group, 10 mice in 3% USMB with 0 Gy, and 12 mice in 3% USMB with 8 Gy. For S1P growth curves, there are five mice in the control group, six mice in the 8 Gy group, five mice in 3% USMB with 0 Gy, and five mice in 3% USMB with 8 Gy. All statistical comparisons are carried out with an unpaired two-tailed t test and compared with the 0 Gy, 0% USMB (Nil) condition at the same time point. Samples from four tumors per condition were labeled. **Error bars** represent standard deviations. Tumor volume doubling time was approximately five to six, 12, eight, and >20 days for control, 8 Gy, 0 Gy with high USMB, and 8 Gy with high USMB treatments, respectively. In contrast, S1P-treated mice experienced minimal growth delay with an approximate tumor doubling time of four, three, eight, and eight days for control, 8 Gy, 0 Gy with high USMB, and 8 Gy with high USMB, respectively. **Error bars** represent SD. ko = knockout; S1P = sphingosine-1-phosphate; wt = wild-type.

and de novo ceramide generation (18). The study also indicated that sphingomyelinase-based hydrolization of sphingomyelin following cell exposure to USMB was linked to neutral sphingomyelinase, while that resulting from radiation was attributed to acid sphingomyelinase. Acid sphingomyelinase is synthesized from the SMPD1 gene and can localize to multiple cellular compartments. In contrast, cells tend to express several different neutral sphingomyelinases (encoded by the SMPD2-4 genes), which are limited to the cytoplasm, and localize to the endoplasmic reticulum or mitochondrial membranes. Both are connected to ceramide production and cell death; acid sphingomyelinase has been predominantly linked to radiation/ultraviolet-induced stress, while neutral sphingomyelinase has been linked to oxidative, hypoxic, or mechanical forms of stressors (38–42). Thus, we posit that statistically nonsignificant increases in ceramide after USMB alone may be related to neutral sphingomyelinase.

Limitations of this study include the following points. First, CD31 MVD assessments cannot differentiate between perfused and nonperfused vessels. While a similar trend in MVD to in vivo 3D power Doppler imaging was noted, future studies should also include a perfusion assay as gold standard histological assessment. Second, whereas 3D Doppler is an ideal and simple imaging modality, it lacks resolution for blood vessel imaging. Thus, future studies should investigate the effects of treatment on capillaries using contrast-enhanced ultrasound or optical imaging. Finally, experiments were balanced for breath and scope, resulting in greater variance for some conditions. While a statistician confirmed the appropriateness of the statistical tests, future studies should further investigate these effects using more subjects per treatment condition.

The results presented here add to the body of work demonstrating the importance of ASMase in radiotherapy and mechanobiology. Numerous questions remain regarding combined USMB and radiation effects and how these alter the tumor microenvironment (7,8). Clinical implementation will require planning to maximize the combinatory effects of radiation and USMB in the lesion-minimizing effects in the path of the radiation and ultrasound fields (13,32,33,43). Effects on tumor growth with fractionated radiotherapy have been examined elsewhere (12). Also to that point, modern technology can focus ultrasound conformally without nearfield effects on tissue. Furthermore, recent technology implementing magnetic resonance imaging–targeting, ultrasound-cavitation feedback, and super-resolution imaging permits microbubble activity to be monitored and modulated to minimize damage. Finally, further work should further optimize radiation and USMB dosage to maximize effects and characterize limits (32,43). This work is the first to demonstrate the involvement of the ASMase-ceramide pathway in mechanotransductive vascular targeting using chemical and genetic approaches to investigate USMB and single-dose radiation.

Funding

This work was supported by the Canadian Cancer Society Research Institute (RG-10-A-700365) and by the Terry Fox Foundation (RA-15) and with funding from the National Institutes of Health (5R01EB017288-04). GJC is a recipient of a University of Toronto James and Mary Davie Chair in Breast Cancer Imaging and Ablation.

Notes

Affiliations of authors: Physical Sciences, Sunnybrook Research Institute, Toronto, ON, Canada (AAM, AH, NL, AG, GJC); Department of Radiation Oncology, Sunnybrook Health Sciences Centre, Toronto, ON, Canada (AEK, AAM, AH, NL, AG, GJC); Departments of Medical Biophysics and Radiation Oncology, University of Toronto, Toronto, ON, Canada (AEK, GJC); Department of Radiology, School of Medicine, Stanford University, Palo Alto, CA (AEK).

The funders had no role in the design of the study; the collection, analysis, or interpretation of the data; the writing of the manuscript; or the decision to submit the manuscript for publication.

We thank Dr. Jarrett Rosenberg (statistician in the Department of Radiology at Stanford University) regarding statistical and data analysis methods. The fibrosarcoma cell line (MCA-129) was obtained from Dr. Richard Kolesnick at the Memorial Sloan-Kettering Institute for Cancer Research, as were the initial colony-forming mice used in this research.

References

1. Hall EJ, Giaccia AJ. *Radiobiology for the Radiologist*. New York: Lippincott Williams and Wilkins; 2006.
2. García-Barros M, Thin TH, Maj J, et al. Impact of stromal sensitivity on radiation response of tumors implanted in SCID hosts revisited. *Cancer Res*. 2010;70(20):8179–8186.
3. Garcia-Barros M, Paris F, Cordon-Cardo C, et al. Tumor response to radiotherapy regulated by endothelial cell apoptosis. *Science*. 2003;300(5622):1155–1159.
4. Truman J-P, García-Barros M, Kaag M, et al. Endothelial membrane remodeling is obligate for anti-angiogenic radiosensitization during tumor radiosurgery. *PLoS One*. 2010;5(8):e12310.
5. El Kaffas A, Al-Mahrouki A, Tran WT, Giles A, Czarnota GJ. Sunitinib effects on the radiation response of endothelial and breast tumor cells. *Microvasc Res*. 2014;92:1–9.
6. El Kaffas A, Giles A, Czarnota GJ. Dose-dependent response of tumor vasculature to radiation therapy in combination with Sunitinib depicted by three-dimensional high-frequency power Doppler ultrasound. *Angiogenesis*. 2013;16(2):443–454.
7. El Kaffas A, Tran W, Czarnota GJ. Vascular strategies for enhancing tumour response to radiation therapy. *Technol Cancer Res Treat*. 2012;11(5):421–432.
8. Fuks Z, Kolesnick R. Engaging the vascular component of the tumor response. *Cancer Cell*. 2005;8(2):89–91.
9. Peña L a, Fuks Z, Kolesnick RN. Radiation-induced apoptosis of endothelial cells in the murine central nervous system: Protection by fibroblast growth factor and sphingomyelinase deficiency. *Cancer Res*. 2000;60(2):321–327.
10. Truman J, Hambardzumyan D, Garcia-Barros M, et al. Basic fibroblast growth factor inhibits radiation-induced apoptosis of endothelial cells by inhibiting acid sphingomyelinase activity. *Radiother Oncol*. 2006;78(2):S74–S74.
11. Mammoto A, Ingber DE. Cytoskeletal control of growth and cell fate switching. *Curr Opin Cell Biol*. 2009;21(6):864–870.
12. Czarnota GJ, Karshafian R, Burns PN, et al. Tumor radiation response enhancement by acoustical stimulation of the vasculature. *Proc Natl Acad Sci U S A*. 2012;109(30):E2033–E2041.
13. El Kaffas A, Czarnota GJ. Biomechanical effects of microbubbles: From radiosensitization to cell death. *Future Oncol*. 2015;11(7):1093–1108.
14. Karshafian R, Tchouala JIN, Al-Mahrouki A, Giles A, Czarnota GJ. Enhancement of radiation therapy by ultrasonically-stimulated microbubbles in vitro: Effects of treatment scheduling on cell viability and production of ceramide. Paper presented at: *2010 IEEE International Ultrasonics Symposium*; October 2010; San Diego, CA.
15. Klinger AL, Pichette B, Sobolewski P, Eckmann DM. Mechanotransductional basis of endothelial cell response to intravascular bubbles. *Integr Biol (Camb)*. 2011;3(10):1033–1042.
16. Mammoto A, Connor KM, Mammoto T, et al. A mechanosensitive transcriptional mechanism that controls angiogenesis. *Nature*. 2009;457(7233):1103–1108.
17. Nofiele JT, Karshafian R, Furukawa M, et al. Ultrasound-activated microbubble cancer therapy: Ceramide production leading to enhanced radiation effect in vitro. *Technol Cancer Res Treat*. 2013;12(1):53–60.
18. Al-Mahrouki A, Karshafian R, Giles A, Czarnota GJ. Bioeffects of ultrasound-stimulated microbubbles on endothelial cells: Gene expression changes associated with radiation enhancement in vitro. *Ultrasound Med Biol*. 2012;38(11):1958–1969.

19. El Kaffas A, Nofiele J, Giles A, Cho S, Liu SK, Czarnota GJ. Dll4-notch signalling blockade synergizes combined ultrasound-stimulated microbubble and radiation therapy in human colon cancer xenografts. *PLoS One*. 2014;9(4):e93888.
20. Al-Mahrouki A, Iradji S, Tran WT, Czarnota GJ. Cellular characterization of ultrasound-stimulated microbubble radiation enhancement. *Dis Model Mech*. 2014;7(3):363–372.
21. Kwok SJJ, El Kaffas A, Lai P, et al. Ultrasound-mediated microbubble enhancement of radiation therapy studied using three-dimensional high-frequency power Doppler ultrasound. *Ultrasound Med Biol*. 2013;39(11):1983–1990.
22. Bonnaud S, Niaudet C, Legoux F, et al. Sphingosine-1-phosphate activates the AKT pathway to protect small intestines from radiation-induced endothelial apoptosis. *Cancer Res*. 2010;70(23):9905–9915.
23. Bonnaud S, Niaudet C, Pottier G, et al. Sphingosine-1-phosphate protects proliferating endothelial cells from ceramide-induced apoptosis but not from DNA damage-induced mitotic death. *Cancer Res*. 2007;67(4):1803–1811.
24. Kim HC, Al-Mahrouki A, Gorjizadeh A, Karshafian R, Czarnota GJ. Effects of biophysical parameters in enhancing radiation responses of prostate tumors with ultrasound-stimulated microbubbles. *Ultrasound Med Biol*. 2013;39(8):1376–1387.
25. Goertz DE, Yu JL, Kerbel RS, Burns PN, Foster FS. High-frequency Doppler ultrasound monitors the effects of antivascular therapy on tumor blood flow. *Cancer Res*. 2002;62(22):6371–6375.
26. Palmowski M, Huppert J, Hauff P, et al. Vessel fractions in tumor xenografts depicted by flow- or contrast-sensitive three-dimensional high-frequency Doppler ultrasound respond differently to antiangiogenic treatment. *Cancer Res*. 2008;68(17):7042–7049.
27. Su J-M, Huang Y-F, Chen HHW, Cheng Y-M, Chou C-Y. Three-dimensional power doppler ultrasound is useful to monitor the response to treatment in a patient with primary papillary serous carcinoma of the peritoneum. *Ultrasound Med Biol*. 2006;32(5):623–626.
28. Chen J-J, Chen J-JJ, Chiang C-S, Hong J-H, Yeh C-K. Assessment of tumor vasculature for diagnostic and therapeutic applications in a mouse model in vivo using 25-MHz power Doppler imaging. *Ultrasonics*. 2011;51(8):925–931.
29. Nico B, Benagiano V, Mangieri D, Maruotti N, Vacca A, Ribatti D. Evaluation of microvascular density in tumors: Pro and contra. *Histol Histopathol*. 2008;23(5):601–607.
30. Hochberg Y, Tamhane AC, eds. *Multiple Comparison Procedures*. Hoboken, NJ: John Wiley & Sons, Inc.; 1987.
31. Kutner MH, Nachtsheim C, Neter J, Li W. *Applied Linear Statistical Models*. New York, NY: McGraw-Hill Irwin; 2005.
32. Czarnota GJ. Ultrasound-stimulated microbubble enhancement of radiation response. *Biol Chem*. 2015;396(6–7):645–657.
33. El Kaffas A, Czarnota GJ. Tumor vascular conundrum: Hypoxia, ceramide, and biomechanical targeting of tumor vasculature. In: Sahgal A, Lo SS, Ma L, Sheehan JP, eds. *Image-Guided Hypofractionated Stereotactic Radiosurgery: A Practical Approach to Guide Treatment of Brain and Spine Tumors*. 1st ed. Boca Raton, FL: CRC Press; 2016:9.
34. Tabas I. Secretory sphingomyelinase. *Chem Phys Lipids*. 1999;102(1–2):123–130.
35. Paliwal S, Mitragotri S. Therapeutic opportunities in biological responses of ultrasound. *Ultrasonics*. 2008;48(4):271–278.
36. Johnson CA, Sarwate S, Miller RJ, O'Brien WD. A temporal study of ultrasound contrast agent-induced changes in capillary density. *Ultrasound Med Biol*. 2010;29(9):1267–1275.
37. Presa N, Gomez-Larrauri A, Rivera I-G, Ordoñez M, Trueba M, Gomez-Muñoz A. Regulation of cell migration and inflammation by ceramide 1-phosphate. *Biochim Biophys Acta Mol Cell Biol Lipids*. 2016;1861(5):402–409.
38. Henry B, Möller C, Dimanche-Boitrel M-T, Gulbins E, Becker KA. Targeting the ceramide system in cancer. *Cancer Lett*. 2013;332(2):286–294.
39. Czarny M, Schnitzer JE. Neutral sphingomyelinase inhibitor scyphostatin prevents and ceramide mimics mechanotransduction in vascular endothelium. *AJP Hear Circ Physiol*. 2004;287(3):H1344–H1352.
40. Czarny M, Liu J, Oh P, Schnitzer JE. Transient mechanoactivation of neutral sphingomyelinase in caveolae to generate ceramide. *J Biol Chem*. 2003;278(7):4424–4430.
41. Marchesini N, Hannun YA. Acid and neutral sphingomyelinases: Roles and mechanisms of regulation. *Biochem Cell Biol*. 2004;82(1):27–44.
42. Pavoine C, Pecker F. Sphingomyelinases: Their regulation and roles in cardiovascular pathophysiology. *Cardiovasc Res*. 2009;82(2):175–183.
43. Briggs K, Al Mahrouki A, Nofiele J, et al. Non-invasive monitoring of ultrasound-stimulated microbubble radiation enhancement using photoacoustic imaging. *Technol Cancer Res Treat*. 2014;13(5):435–444.